Nanoscale

Accepted Manuscript

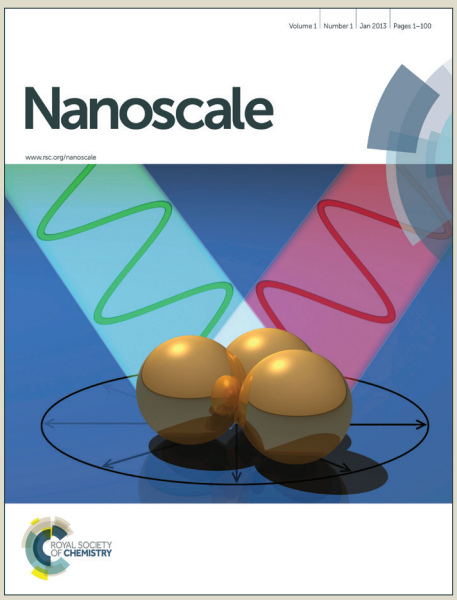

ROYAL SOCIETY OF CHEMISTRY

www.rsc.org/nanoscale

Cite this: DOI: 10.1039/c0xx00000x

www.rsc.org/xxxxxx

ARTICLE TYPE

Improving the sensing performance of double gold gratings by oblique incident light†

Feifei Wu, Lingxiao Liu, Lei Feng, Daren Xu and Nan Lu*

Received (in XXX, XXX) Xth XXXXXXXXX 20XX, Accepted Xth XXXXXXXXX 20XX

DOI: 10.1039/b000000x

Here we demonstrate a simple method to improve the plasmonic sensing performance of gold gratings. The gratings consist of periodic polymer gratings covered with gold layer, created by nanoimprint lithography and metal deposition. We investigated the effect of gold thickness and the incident angles on the plasmonic sensing performance. With the optimized gold layer, the full width at half maximum of this grating was reduced to 40% by using the oblique incident light instead of the normal incident light. A maximum value of the figure of merit at oblique incidence is 12, which is doubled of the one at normal incidence.

1 Introduction

Surface plasmon polaritons (SPP) are electromagnetic waves propagating at the interface between a metal and a dielectric material.[1] In the perpendicular direction, surface plasmon are evanescent waves whose electric field amplitude decays exponentially into each medium with increasing distance from the interface.[2] A strong absorption of the electromagnetic waves appears when the oscillations of the conductor's electron plasma couple to the electromagnetic fields. This peak position is very sensitive to the refractive index change of the surrounding medium of the metal film.[3, 4] A change in the refractive index of the surrounding environment results in a change in the propagation constant of the surface plasmon, which can be monitored by the shift of the peak positions of surface plasmon resonances (SPR).[5] These unique properties of SPP can be used for chemical sensing[6-9]. Over the past decades, SPR sensors based on the peak shift of SPR have been widely investigated and applied in many fields, such as food quality[10,11], medical diagnostics[12-14], environmental monitoring[15,16], renewable energy[17] and photovoltaic devices[18, 19].

Sensitivity (S) and figure of merit (FOM) are two main performance characteristics for evaluating SPR sensors.[20, 21] S is defined as the ratio of resonant wavelength shift $\Delta\lambda_{res}$ to the variation of surrounding refractive index Δn_s: $S = \frac{\Delta\lambda_{res}(nm)}{\Delta n_s(RIU)}$, where RIU means refractive index unit. FOM is considered as an important parameter in verifying nanosensor. It is defined as the ratio of the refractive index sensitivity to the resonance width $\Delta\lambda$: $FOM = \frac{S(nm \cdot RIU^{-1})}{\Delta\lambda(nm)}$. The sensing performance can be improved by increasing the sensitivity and reducing the resonance peak width, which can be described as full width at half maximum (FWHM).

To achieve better sensing performance, researchers mainly focus on the two approaches. (1) Confine or localize the light into a small area to get high sensitivity. The enhanced electromagnetic field localized at the spatial area can be exposed to surrounding medium directly and be accessible by molecular species. Some of the simple nanostructures are more suitable for refractive index sensors, including nanoholes[22-24], nanorings[25-27], nanodisks[28-31] and so on. Meanwhile, a number of coupled metallic nanostructures were reported due to their enhanced electromagnetic fields are sensitive for detecting the refractive index differences, including gold disk trimers[32], gold nanoring dimers[33], closely packed nanodisk clusters[34]. (2) Couple different resonance modes (e.g. localized surface plasmon resonance, propagating surface plasmon resonance, Wood's anomaly) into one nanostructure unit to obtain narrow peak width and increase the FOM value. Shen *et al.*[35] presented a gold mushroom array, which looks like a periodic array of mushrooms grown on a gold film with a periodic array of holes. The resonance mode of this array couples a localized surface plasmon resonances with Wood's anomaly[36] to obtain narrower peaks, leading to high sensitivity and high FOM. Zhan *et al.*[23] reported the nanohole quadrumer system performed higher FOM, which surpassed the value achieved with conventional nanoparticle oligomers. They adjusted the geometrical parameters of the nanohole clusters to obtain strong mode coupling between either two antiparallel dipolar modes or dipole–quadruple modes in the nanohole quadrumer. Moreover, following the guidance of theoretical simulation, Evlyukhin *et al.*[37] demonstrated a detuned electric dipoles, which included a pair of electrical dipolar scatterers resonating at different frequencies. And a high FOM of 200 was achieved by controlling the length of each dipole and the distance between the two dipoles. However, most of these works need complex nanostructures for improving the sensing performance. Generally, the fabrication of complex structures cannot avoid expensive equipments to maintain the high accuracy and they are

always time-consuming[23, 38, 39]. So the applications of these complex nanostructures in actual detection are limited.

As one of the simplest nanostructures, metal grating has been widely investigated. SPP is produced and propagated along with the grating when the light illuminate on the metal grating surfaces directly.[40] However, their waveguide coupling mode results in a wide peak and low sensitivity, leading to a poor sensing performance. Recently, Tsai *et al.*[41] reported that the small oblique incidence induced a resonant coupling between metal surface and substrate surface plasmon modes of periodic gold nanoslits. And this resonant coupling increased the sensitivity and FOM of the arrays. Lee *et al.*[42] reported there existed enhanced Fano resonance in capped gold nanoslit arrays. The cavity resonance mode in nanoslits and surface plasmon resonance mode on periodic metallic surface formed the enhanced Fano coupling, resulting in ultrasmall linewidth. Usually, high FOM can be obtained on the gratings with narrow slit width because slit width is related to the linewidth of spectra[43]. But the high accuracy is needed for the fabrication of narrow slit, which limits the applications of the narrow slits.

In this paper, we fabricated double gold gratings of wide slit with nanoimprint lithography (NIL) and metal thermal evaporation. Nanoimprint lithography is more efficient than serial writing techniques. With the optimized thickness of gold layer, the plasmonic sensing performance is highly improved by using the oblique incident light instead of the normal light.

2 Experimental Section

2.1 Materials

All chemicals including polymethylmethacrylate (PMMA, molecular weight Mw = 97000) and tridecafluoro-1,1,2,2-tetrahydrooctyl-trichlorosilane (FDTS), were purchased from Sigma-Aldrich Inc.. One-side polished n-type (100) oriented Si wafers with a resistivity of 0.008–0.02 Ω·cm were purchased from GRINM Advanced Materials Co., Ltd., Beijing, China. NIL was performed in a clean room and the other processes were carried out in a standard chemistry laboratory. All glassware was washed with *Potassium dichromate - Sulfuric acid lotion* before use.

2.2 Preparation of double gold nanogratings

The silicon substrates were treated according to the paper[44]. A PMMA layer of 100 nm was spin-coated onto the silicon wafer followed by a baking at 90 ℃ for 10 min to remove residual solvent. The imprinting and metal deposition process were carried out as described elsewhere[45].

2.3 Characterization

The morphology of the samples was characterized by atomic force microscopy (AFM, Digital Instrument, Santa Barbara, CA) running in tapping mode and scanning electron microscope (SEM, HITACHI SU8020 field emission scanning electron microscope). Reflectance spectra were recorded on R1-A-UV series spectroscopy meter (Shanghai Ideaoptics Technology Co., Ltd., China).

To examine the performance of the double gold gratings as a refractive index sensor, we measured the zero-order reflectance spectra at oblique incident angles. The index sensitivity was determined by immersing the same gratings in the sucrose aqueous solutions of different concentrations. The concentrations of sucrose aqueous solutions were 0, 5, 10, 15, 20, 25, 30, 40, 50 and 60 wt%, and the corresponding refractive indices were 1.3330, 1.3372, 1.3478, 1.3556, 1.3639, 1.3740, 1.3812, 1.4000, 1.4200 and 1.4419, respectively. After the reflectance spectrum was recorded, the sample was taken out, rinsed with water and dried with flowing nitrogen. This procedure was repeated and three measurements were made at each refractive index.

2.4 Finite-difference time-domain (FDTD) simulation

Lumerical FDTD Solutions software was used to simulate the field intensity and distribution near the nanograting structure.[46] The dielectric coefficients of Au and Si were obtained from Palik's handbook.[47] The mesh size is 1 nm in all the three dimensions.

3 Results and Discussion

3.1Fabrication of the double gold gratings

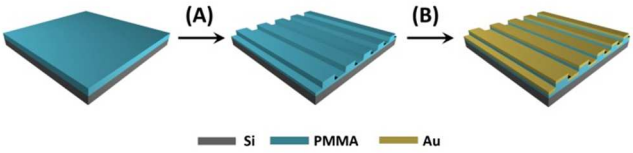

Figure 1. Scheme illustration of the fabrication process. (A) Taking NIL on PMMA layer; (B) Thermal evaporating Au layer.

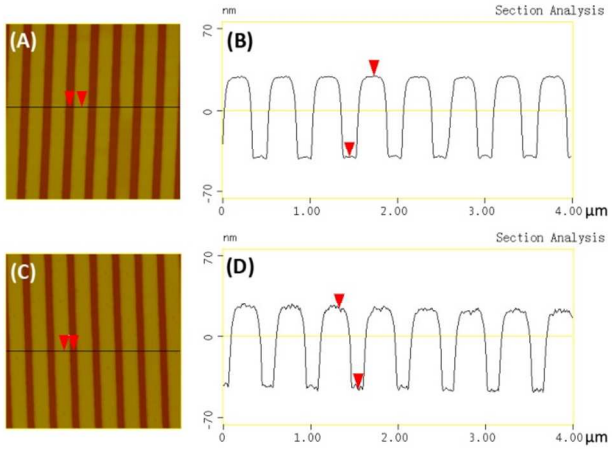

Figure 2. (A, B) AFM topography image and cross-sectional analysis of PMMA gratings; (C,D) AFM topography image and cross-sectional analysis of PMMA gratings covered with 20 nm Au. Period: 500 nm, height: 70 nm. The size of AFM images are 4 μm × 4 μm.

Figure 1 shows the scheme illustration of fabrication process. The process consists only two major steps: imprinting (Figure 1A) and thermal evaporating metal (Figure 1B). Prior to taking NIL process, a monolayer of FDTS was self-assembled on the Si stamp as releasing agent, which provided a low surface energy in order to facilitate the separation of the stamp and the resist.[48, 49] A spin-coated 100 nm PMMA layer on the Si substrate was used as resist layer for NIL. After the NIL process, gold was deposited on the PMMA gratings directly by thermal evaporation process. The evaporation rate of gold was ca. 5 nm/min, which was monitored by quartz crystal microbalance. As revealed in Figure 2A and 2B,

Cite this: DOI: 10.1039/c0xx00000x

www.rsc.org/xxxxxx

ARTICLE TYPE

the silicon stamp used for NIL is ca. 500 nm in period (210 nm line and 290 nm space) and ca. 70 nm in depth. The size of the double gold grating (Figure 2C and 2D) is similar with that of the PMMA grating. We randomly chose 25 points (each of 14 nm^2), on the gratings before and after depositing gold to calculate the surface roughness. The root mean square of the roughness changes from 2.3 nm of PMMA grating to 3.0 nm of gold grating in average, which means the surface of gold grating is a little rougher than that of PMMA grating. It's obviously observed from the corresponding AFM cross-sectional analysis (Figure 2B and 2D).

To investigate the effect of gold thickness on sensing performance, we deposited 23, 44, 65, 92 nm gold layer on the PMMA gratings (named as S1, S2, S3 and S4) respectively. The SEM images with titled-view (45°) of PMMA gratings coated with different Au thickness are shown in Figure 3. It reveals that there are some small slits between the top and the bottom gold gratings, which were formed in the metal thermal evaporation procedure. The slits become smaller and less when the thickness of gold increases. When the thickness of deposited gold was higher than the groove depth, the slits disappeared and gold layer covered the PMMA grating completely as shown in Figure 3D. The corresponding side-view SEM images illustrated as the insets in Figure 3A-3D show that the gap between two metal layers became smaller as the metal thickness increased. SEM images with titled-view (45°) of these double gold gratings are parallell to the grating direction (detailed in Figure S1), which show that the arrays kept the same period and the roughness were similar as that in Figure 2D.

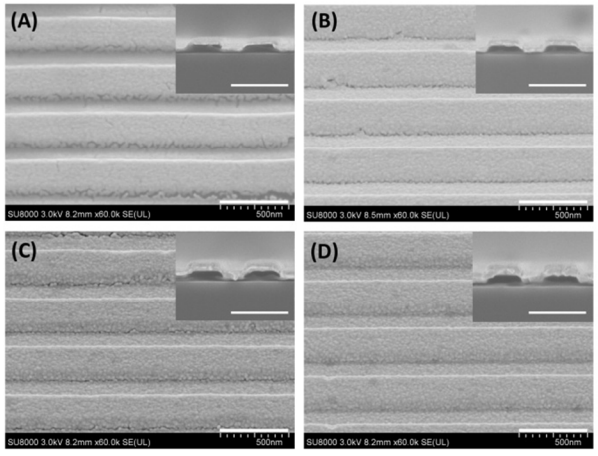

Figure 3. SEM images with titled view (45°) of PMMA gratings coated with gold films of different thickness. The metal thickness of (A) - (D): 23, 44, 65, 92 nm and the inset images in (A) - (D) are the corresponding cross sectional SEM images. Scale bar: 500 nm.

3.2 The optimization of gold thickness for plasmonic sensing

According to Bragg condition, when the incident light illuminate on the metal surface directly, the scattered waves interfere constructively. The Bloch wave exists in the periodic nanostructures and is scattered by the periodic grooves. So the Bloch wave surface plasmon polariton (SW-SPP) occurs when the Bloch wave satisfied the Bragg condition. .[50] The condition for a 1D array is dominated by the period and can be described by :

$$\lambda_{SPR}(n,i) = \frac{P}{i}\mathrm{Re}\{(\frac{\varepsilon_m n^2}{\varepsilon_m + n^2})^{1/2}\} \qquad (1)$$

where n is the refractive index of surrounding medium, i is the resonant order, P is the period of the nanostructure and ε_m is the dielectric constant of metal. For the gold array with period of 500 nm, when n changes from 1.0 to 1.5, the resonant wavelength locates at the visible and near-infrared area, which is beneficial to be monitored. However, the thickness of metal layers affect the intensity between the BW-SPP and the cavity resonances in the double gold gratings.

We measured the reflectance spectra of S1-S4 in air under normal illumination as shown in Figure 4A-4D. The black and red curves are the simulated and experimental spectra, respectively. The experimental spectra were collected at white light instead of polarized light which was used in the simulated spectra, leading to a small deviation between the experimental and simulated spectrum (detailed in Figure S2 of supporting information). And the deviation of the groove width and the shape of the grating edge influenced the peak shift and the peak width.[43] As shown in Figure 4E-4H, the increased thickness of gold supports the increased degree of localized electromagnetic field between the top and bottom gold gratings. As the thickness of gold increases from 23 nm to 65 nm, the electromagnetic enhancement area expands on the edges of both the top gold layer and the bottom gold layer and the intensity increases, which are shown in Figure 4E-4G. But as shown in Figure 4H, the electromagnetic enhancement area locates on the edge of the top gold layer and the interface of the PMMA/bottom gold layer, and the intensity decreases compared with Figure 4G. So when the thickness of gold layer is close to the height of PMMA groove, the enhancement area of electromagnetic field is the largest and the intensity is the biggest.

Reflection spectra of sample S1-S4 at normal light with different concentrations of sucrose aqueous solutions are shown in Figure S3. When the concentration of sucrose aqueous solution increases, the refractive index of the surrounding medium near the gold surface increases and the resonant wavelength red-shifts according to equation(1). The sensitivity and FOM of sample S1-S4 are shown in Table 1. With the increase of gold thickness from sample S1 to S4, the sensitivity initially increased and then decreased. The maximum of sensitivity (448.9 nm/RIU) was achieved when the thickness of gold was 65 nm, which was the closest to the height of PMMA grating among these samples. The variation trend in sensitivity (Table 1) agrees well with that in localized degree of electromagnetic field (Figure 4E-4H), which

corresponds to the reported results[51]. Due to the weak probing peak and intensity distinction, sample S1 exhibits the lowest sensitivity and the narrowest FWHM. For sample S2-S4, the FWHM decreases with increasing the thickness of gold layer due to the localized degree of electromagnetic field on the metal surface, and S3 performs the best sensing capability among them.

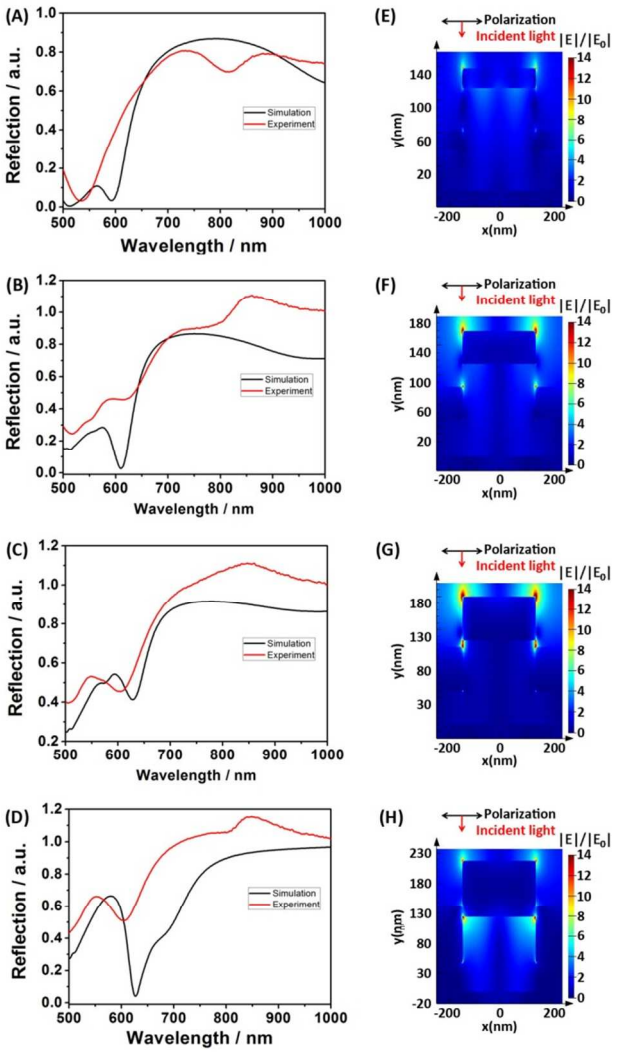

Figure 4. (A)~(D): The simulated (black curve) and experimental (red curve) reflectance spectra at normal incident angle corresponding to S1-S4; (E)~(H): Calculated electromagnetic field distribution of the samples under a series of resonance wavelengths corresponding to the dips of (A)-(D): (E) 593, (F) 610, (G) 620 and (H) 626 nm.

Table 1 The sensitivity and FOM of different samples at normal incidence angle.

sample	Sensitivity (nm / RIU)	FWHM* (nm)	FOM (RIU^{-1})
S1	244.3	31.14	7.8
S2	359.6	105.20	3.4
S3	448.9	78.47	5.7
S4	321.8	64.83	5.0

(NOTE: **FWHM*** is the average value of the full-width at half maximum for period dips with different solutions.)

3.3 Effect of the incident angle on plasmonic sensing performance

To investigate the effect of incident angle on plasmonic sensing performance, we measured the reflectance spectra of the gold grating coupler at oblique incident angles with white light and the plane of incidence was perpendicular to the gratings. We chose sample S3 as model due to its best sensing performance at normal incidence. And the other samples were discussed in detail hereafter. The experimental zero-order reflectance spectrum of S3 at oblique incidence in air is shown in Figure 5. At the air/gold interface, the larger incident angle resulted in the decreasing of reflection intensity because the light diffraction increased with increasing the incident angle[52]. Meanwhile, the application of white light results in the overlapping orders at zero-order reflectance spectrum. According to the grating equation, the longer wavelength exhibits smaller diffraction order at larger incidence angle. So the dip positions of the samples red-shift as the incident angle increases, which is shown in Figure 5. The reflectance spectra of sample S1, S2 and S4 are detailed in Figure S4 and these samples have the same variation trend in reflectivity with the variation of the incident angle, which is similar to that of S3. Taking the changes of wavelength and intensity into consideration, incident angle of 20°, 25°, 30° were chosen to investigate the correlation of the sensing performance and the incident angle. The calculated distribution of electromagnetic field at different incident angles are shown in Figure 6A-6C and the TM-polarized light and incident angle versus the structures is depicted in the inset. It is clearly that the oblique incident light breaks the symmetry of the distributions of enhanced electromagnetic field. Compared with the spectra at normal incident light, shown in Figure 4G, the distribution of enhanced electromagnetic field locate at both the top and bottom gold grating. The resonance coupling of top and bottom SPR modes makes a resonant system which generated Fano-like resonances with asymmetric spectral profiles, leading to more SPR energy and narrow resonant linewidth.

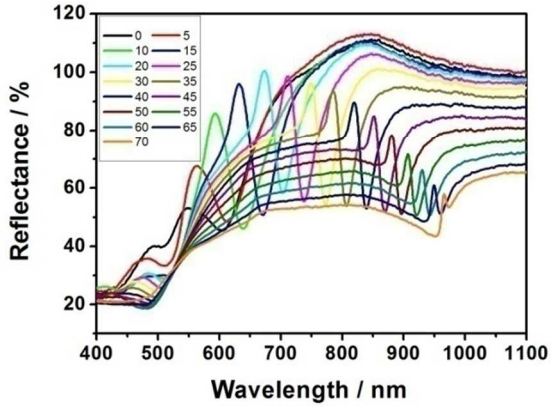

Figure 5. Reflection spectra of sample S3 in air at different incident angles with white light.

Cite this: DOI: 10.1039/c0xx00000x

www.rsc.org/xxxxxx

ARTICLE TYPE

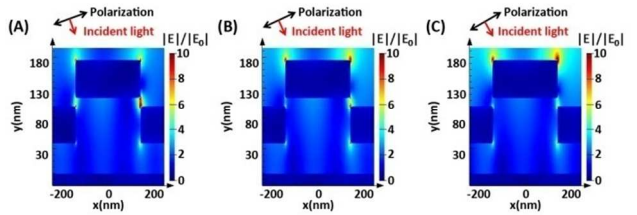

Figure 6. (A-C) The distribution of electromagnetic field of sample S3 with incident angle of 20°, 25° and 30° under a series of resonance wavelengths: (A)720, (B)755 and (C)785 nm in air, respectively.

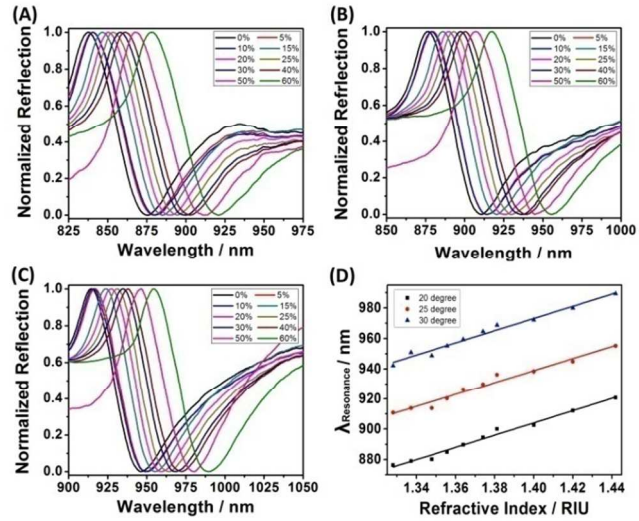

Figure 7. (A-C) Experimental reflection spectra of sample S3 with different concentrations of sucrose aqueous solution at the incident angle of 20°, 25° and 30°, respectively. (D) The wavelength changes against the refractive index of the surrounding medium. The slopes of the fitting curves show that refractive index sensitivities corresponding to (A)-(C) were 403.9, 396.1 and 399.0 nm/RIU.

In order to investigate the effect of oblique incident light on sensing performance, wavelength sensitivity of sample S3 were measured under different concentrations of sucrose aqueous solutions with the refractive indices from 1.3330 to 1.4419. And the experimental reflection spectra at the incident angle of 20°, 25° and 30° were shown in Figure 7A-7C, respectively. When the surrounding medium was changed from water to sucrose aqueous solutions, the Fano-like resonant wavelength red-shifted at each oblique incident angle. The wavelength change against the refractive index of the surrounding medium is shown in Figure 7D. For incident angle at 20°, 25° and 30°, the slopes of the fitting curves show that refractive index sensitivities were 403.9, 396.1 and 399.0 nm/RIU (detailed in Table 2), respectively. The wavelength sensitivity decreases ca. 0.12 times for oblique incidence compared with normal incidence. Although the enhanced electromagnetic field locating at both the top and bottom gold layer for oblique incidence, the field intensity is lower than that for normal incidence. Furthermore, the SPR mode on the top layer is much more sensitive to the change of surrounding medium. So the wavelength sensitivity of oblique incidence is not as high as that of normal incidence. However, the FOM values of oblique incidence are 0.7~1.1 times higher than that of normal incidence as a result of the great improvement of FWHM, which is reduced to 40% of the one at normal incident light.

Compared Table 1 and Table 2, the sensitivity of sample S1 and the FOM value of sample S2 with thinner gold layers are ca. 1.5 times and 2.1 times higher at oblique incident light, respectively. This improvement of sensing performance is the contribution of the enhancement of the electromagnetic field with oblique incident light. For sample S4, the FOM is almost 2 times of the one achieved with normal light because of the decreased FWHM at oblique incident light. The above investigation indicates that the oblique incident light can be applied for improving the sensing performance of double gold gratings. And these uniform substrates are suitable candidates for sensing applications.

4 Conclusions

In summary, we fabricated the double gold gratings of wide slit by the combination of nanoimprint lithography and metal thermal evaporation. The wavelength sensitivity was increased by increasing the thickness of the metal layer at normal incident light. Using the oblique incident light can improve the sensing performance of double gold gratings apparently. With the optimized thickness (65 nm) of gold layer, the linewidth of the double grating was reduced to 40% and the FOM of this grating was doubled by using the oblique incident light instead of the normal incident light. Moreover, using the white light instead of the polarized light is beneficial for sensing application. Therefore, this is a simple and efficient way to enhance the sensing performance of double gold grating arrays by measuring at oblique incidence, which can be used as a candidate for label-free sensor.

Acknowledgement

This work was supported by the National Natural Science Foundation of China (No. 21273092) and the National Basic Research Program of China (No. 2009CB939701).

Notes and References

State Key Laboratory of Supramolecular Structure and Materials, College of Chemistry, Jilin University, Changchun 130012, P. R. China. E-mail: luenan@jlu.edu.cn; Fax: +86-431-85168477; Tel: +86-431-85168477.

†Electronic Supplementary Information (ESI) available: [SEM

images with titled (45°) view of S1-S4; Simulated spectra of

Table 2 The refractive index sensing capability of different samples at oblique incident angle.

sample	20°		25°		30°	
	S(nm / RIU)	FOM(RIU^{-1})	S(nm / RIU)	FOM(RIU^{-1})	S(nm / RIU)	FOM(RIU^{-1})
S1	353.8	8.7	374.7	9.2	343.5	9.1
S2	373.8	10.1	378.1	10.7	365.2	10.6
S3	403.9	11.9	396.1	12.1	399.0	9.7
S4	371.8	11.6	358.9	10.1	322.8	7.6

double gold gratings under different polarized lights; Refractive index sensing of gold grating at normal light with different sucrose aqueous solutions concentrations; Reflection spectra of gold grating in air using different incidence angles]. See DOI: 10.1039/b000000x.

1 K. M. Mayer and J. H. Hafner, *Chem. Rev.* 2011**, 111**, 3828-3857.
2 L. S. Jung, C. T. Campbell, T. M. Chinowsky, M. N. Mar and S. S. Yee, *Langmuir* 1998**, 14**, 5636-5648.
3 H. X. Xu and M. Kall, *Sens. Actuators. B* 2002**, 87**, 244-249.
4 J. N. Anker, W. P. Hall, O. Lyandres, N. C. Shah, J. Zhao and R. P. Van Duyne, *Nat. Mater.* 2008**, 7**, 442-453.
5 J. Homola, *Anal. Bioanal. Chem.* 2003**, 377**, 528-539.
6 A. Shiohara, J. Langer, L. Polavarapu and L. M. Liz-Marzan, *Nanoscale* 2014**, 6**, 9817-9823.
7 J. Homola, S. S. Yee and G. Gauglitz, *Sens. Actuators. B* 1999**, 54**, 3-15.
8 E. Kazuma and T. Tatsuma, *Nanoscale* 2014**, 6**, 2397-2405.
9 P. Jia and J. Yang, *Nanoscale* 2014**, 6**, 8836-8843.
10 P. D. Patel, *J. Aoac Int.* 2006**, 89**, 805-818.
11 N. Tawil, E. Sacher, R. Mandeville and M. Meunier, *Analyst* 2014**, 139**, 1224-1236.
12 B. Cherif, A. Roget, C. L. Villiers, R. Calemczuk, V. Leroy, P. N. Marche, T. Livache and M. B. Villiers, *Clin. Chem.* 2006**, 52**, 255-262.
13 T. Riedel, C. Rodriguez-Emmenegger, A. de los Santos Pereira, A. Bedajankova, P. Jinoch, P. M. Boltovets and E. Brynda, *Biosens. Bioelectron.* 2014**, 55**, 278-284.
14 X. Guo, *J. Biophotonics* 2012**, 5**, 483-501.
15 S. Zeng, D. Baillargeat, H.-P. Ho and K.-T. Yong, *Chem. Soc. Rev.* 2014**, 43**, 3426-3452.
16 R. Wang, W. Wang, H. Ren and J. Chae, *Biosens. Bioelectron.* 2014**, 57**, 179-185.
17 E. Ozbay, *Science* 2006**, 311**, 189-193.
18 H. A. Atwater and A. Polman, *Nat. Mater.* 2010**, 9**, 205-213.
19 H. Wei and H. Xu, *Nanophotonics* 2012**, 1**, 155-169.
20 L. J. Sherry, S. H. Chang, G. C. Schatz, R. P. Van Duyne, B. J. Wiley and Y. N. Xia, *Nano Lett.* 2005**, 5**, 2034-2038.
21 J. Homola, *Surface Plasmon Resonance Based Sensors*; Springer:Berlin, Germany, 2006, p45-p67
22 T. Sannomiya, O. Scholder, K. Jefimovs, C. Hafner and A. B. Dahlin, *Small* 2011**, 7**, 1653-1663.
23 Y. Zhan, D. Y. Lei, X. Li and S. A. Maier, *Nanoscale* 2014**, 6**, 4705-4715.
24 X. Zhang, Z. Li, S. Ye, S. Wu, J. Zhang, L. Cui, A. Li, T. Wang, S. Li and B. Yang, *J. Mater. Chem.* 2012**, 22**, 8903-8910.
25 E. M. Larsson, J. Alegret, M. Kall and D. S. Sutherland, *Nano Lett.* 2007**, 7**, 1256-1263.
26 A. R. Halpern and R. M. Corn, *ACS Nano* 2013**, 7**, 1755-1762.
27 C. Huang, J. Ye, S. Wang, T. Stakenborg and L. Lagae, *Appl. Phys. Lett.* 2012**, 100**, 173114(4pp).
28 Y.-C. Chang, S.-M. Wang, H.-C. Chung, C.-B. Tseng and S.-H. Chang, *ACS Nano* 2012**, 6**, 3390-3396.
29 S. W. Lee, K. S. Lee, J. Ahn, J. J. Lee, M. G. Kim and Y. B. Shin, *ACS Nano* 2011**, 5**, 897-904.
30 A. E. Cetin and H. Altug, *ACS Nano* 2012**, 6**, 9989-9995.
31 Y. C. Chang, H. C. Chung, S. C. Lu and T. F. Guo, *Nanotechnology* 2013**, 24**, 095302(7pp).
32 V. K. Lin, S. L. Teo, R. Marty, A. Arbouet, C. Girard, E. Alarcon-Llado, S. H. Liu, M. Y. Han, S. Tripathy and A. Mlayah, *Nanotechnology* 2010**, 21**, 305501(7pp).
33 C. Y. Tsai, J. W. Lin, C. Y. Wu, P. T. Lin, T. W. Lu and P. T. Lee, *Nano Lett.* 2012**, 12**, 1648-1654.
34 J. B. Lassiter, H. Sobhani, J. A. Fan, J. Kundu, F. Capasso, P. Nordlander and N. J. Halas, *Nano Lett.* 2010**, 10**, 3184-9.
35 Y. Shen, J. Zhou, T. Liu, Y. Tao, R. Jiang, M. Liu, G. Xiao, J. Zhu, Z. K. Zhou, X. Wang, C. Jin and J. Wang, *Nat. Commun.* 2013**, 4**, 2381(9pp).
36 R. W. Wood, *Proceedings of the Physical Society of London* 1902**, 18**, 269-275.
37 A. B. Evlyukhin, S. I. Bozhevolnyi, A. Pors, M. G. Nielsen, I. P. Radko, M. Willatzen, and O. Albrektsen, *Nano Lett.*, 2010, **10**, 4571-4577.
38 Y. Francescato, V. Giannini, and S. A. Maier, *ACS Nano*, 2012, **6**, 1830-1838.
38 C. Valsecchi and A. G. Brolo, *Langmuir*, 2013, **29**, 5638-5649.
40 H. Raether, *Surface Plasmons on Smooth Surfaces and Rough Surface and on Gratings*; Springer: Berlin, Heidelberg, 1988.
41 W. S. Tsai, K. L. Lee, M. Y. Pan and P. K. Wei, *Opt. Lett.* 2013**, 38**, 4962-4965.
42 K. L. Lee, J. B. Huang, J. W. Chang, S. H. Wu and P. K. Wei, *Sci. Rep.* 2015**, 5,** 8547(9pp).
43 K. L. Lee, P. W. Chen, S. H. Wu, J. B. Huang, S. Y. Yang and P. K. Wei, *ACS Nano* 2012**, 6**, 2931-2939.
44 F. Wu, G. Shi, H. Xu, L. Liu, Y. Wang, D. Qi and N. Lu, *ACS Appl. Mater. Interfaces* 2013**, 5**, 12799-12803.
45 S. Shi, N. Lu, Y. Lu, Y. Wang, D. Qi, H. Xu and L. Chi, *ACS Appl. Mater. Interfaces* 2011**, 3**, 4174-4179.
46 L. Solutions, Inc., https://www.lumerical.com/, accessed:

Cite this: DOI: 10.1039/c0xx00000x

www.rsc.org/xxxxxx

ARTICLE TYPE

August, 2014.

47 E. D. Palik, *Handbook of Optical Constants of Solids,* Academic Press: Orlando, FL, 1985.

48 G. Y. Jung, Z. Y. Li, W. Wu, Y. Chen, D. L. Olynick, S. Y. Wang, W. M. Tong and R. S. Williams, *Langmuir* 2005**, 21**, 1158-1161.

49 B. Dong, N. Lu, M. Zelsmann, N. Kehagias, H. Fuchs, C. M. S. Torres and L. Chi, *Adv. Funct. Mater.* 2006**, 16**, 1937-1942.

50 S.-H. Chang, S. K. Gray and G. C. Schatz, *Opt. Express* 2005**, 13**, 3150-3165.

51 M. Konig, M. Rahmani, L. Zhang, D. Y. Lei, T. R. Roschuk, V. Giannini, C. W. Qiu, M. Hong, S. Schlucker and S. A. Maier, *ACS Nano* 2014, **8**, 9188-9198.

52 J. Homola, I. Koudela and S. S. Yee, *Sens.Actuators. B* 1999, **54**, 16-24.